metals

Article

A Particle Size Distribution Model for Tailings in Mine Backfill

Zongnan Li [1,2,3], Lijie Guo [1,3,*], Yue Zhao [1,3], Xiaopeng Peng [1,3] and Khavalbolot Kyegyenbai [4]

1 Beijing General Research Institute of Mining and Metallurgy, Beijing 100160, China; lizongnan@bgrimm.com (Z.L.); zhaoyue@bgrimm.com (Y.Z.); pengxiaopeng@bgrimm.com (X.P.)
2 School of Civil and Resources Engineering, University of Science and Technology Beijing, Beijing 100083, China
3 National Centre for International Research on Green Metal Mining, Beijing 102628, China
4 School of Geology and Mining Engineering, Mongolian University of Science and Technology, Ulaanbaatar 210646, Mongolia; khavalbolot@must.edu.mn
* Correspondence: guolijie@bgrimm.com

Abstract: With the increasing awareness of sustainable mining, the cement tailings backfill (CTB) method has been developed rapidly over the past decades. In the CTB technique, the two main mechanical properties engineers were concerned with are the rheological properties of CTB slurry and the resulting CTB strength after curing. Particle size distribution (PSD) of tailings material or PSD of the slurry is a significant factor that highly influences the rheological of CTB slurry and the strength performance of CTB. However, the concentrically partial size distribution curve and existing mathematical model could not represent the PSD of tailings material. In this study, a mathematical model for the particle size distribution of mine tailings was established using three model coefficients *A B* and *K*, which mainly reflect the characteristics of particles from three aspects respectively, the average size of particles, the proportion of the coarse or the fine parts of particles, and the distribution width of particles; meanwhile, an optimal coefficient solution method based on error analysis is given. Twelve tailing materials sourced from metal mines around China were used for the model establishment and validation. The determination coefficient of error analysis (R^2) for all twelve modeled PSD lognormal curves was more significant than 0.99, and the modeled PSD lognormal curves are highly consistent with the determined particle size distribution curve.

Keywords: backfill; tailings; particle size distribution; metal mine; log-sigmoid

Citation: Li, Z.; Guo, L.; Zhao, Y.; Peng, X.; Kyegyenbai, K. A Particle Size Distribution Model for Tailings in Mine Backfill. *Metals* **2022**, *12*, 594. https://doi.org/10.3390/met12040594

Academic Editor: Antoni Roca

Received: 24 February 2022
Accepted: 29 March 2022
Published: 30 March 2022

1. Introduction

With the increasing awareness of sustainable mining, the cement tailings backfill (CTB) method has been developed rapidly over the past decades [1–4]. Cement tailings backfill is a technology that assists waste management and mitigates the mine environment from being hazardous by utilizing tailings (or other waste materials) to underground mined voids resulting from underground mine operations [5–8]. It somehow performs as both a support system or an underground working platform to improve the underground mine stability and promote ore extraction [9–12]. The cement tailings backfill is normally mixed to a high-density slurry with a non-settling character, consisting of a low cementitious material content, mine tailings as aggregate, and processed mine water, which could be gravity-transferred or facile pumping into mined cavities [13–16]. After placing CTB slurries in mined cavities, it could then be consolidated and cured to a designed period to achieve particular strength for further mine exaction [17–20].

Tailings used for filling in mines are usually obtained through the beneficiation process, and their particle size range varies according to different beneficiation processes [21–23]. Generally, the tailings produced by the flotation process for copper, lead-zinc, gold, and other raw ores can reach about 80% below 37 µm [24]. The tailings produced by the magnetic separation and gravity separation process are relatively coarse for iron ore, tin ore, etc. According to the 74 μm boundary, the coarse particle part above can account up for about 60% [25,26].

Over the past few decades, due to the low operating costs and well-performed mechanical performance compared with other backfilling methods, CTB technology has been increasingly applied in the mining industry [27–29]. In the CTB technique, the two main mechanical property engineers were concerned with are the rheological properties of CTB slurry and the resulting CTB strength after curing [30–34]. The governing factors of CTB rheological and strength performance have been well documented in the literature [35–38] (e.g., physical and chemical properties of the tailings, chemical composition and content of the mixing water, binder type, and content, the CTB mix design, and in situ curing conditions for strength performance only).

Particle size distribution (PSD) of tailings material or PSD of the slurry is a significant factor that highly influences the rheological and strength performance of CTB [29–31]. Conventionally, there are two forms: interval distribution and cumulative distribution, representing material PSD. Interval distribution, also known as differential distribution or frequency distribution, represents the percentage content of particles in a series of particle size ranges; cumulative distribution represents the percentage content of particles less than specific particle size [37,39]. As the cumulative distribution curve can easily make the cumulative proportion of particles smaller than a specific size, it is widely used in the mine backfill [36,37,39–41]. On the PSD curve, the coarse and fine characteristics of a specific backfill tailing material can be approximately reflected by choosing some points. Such common representative points are usually d_{30}, d_{50}, d_{60}. Here, the symbol d represents the particle size, and the number subscript represents the proportion smaller than the particle size. For example, d_{10} represents a particle size with a cumulative volume fraction less than 10%.

Conventionally, researchers often use these representative points to represent tailing PSD in investigating the relationship between the tailings' PSD with the rheological and strength performance of CTB to solve the problems encountered in CTB slurry transportation underground support [42–44]. Therefore, it is of great significance to study the particle distribution characteristics of tailings. However, the conventional PSD curve is not easy enough to describe the characteristics of particle distribution entirely because the curve is only a collection of scattered points and the selected representative points are random to some extent, i.e., there is no certain equivalent size that can represent the whole particle group features in a conventional PSD curve. Thus, it is of great significance to study the full-size description method of tailings.

Fredlund et al. [45–47] established a mathematical equation representing soil particle size distribution. However, Fredlund's model mainly focuses on naturally grained soils and could not represent the particle size distribution of artificial mine tailings. In addition, in Fredlund's model, five model coefficients are required to represent the PSD, including the initial breaking point of the PSD curve, the steepest slope of the curve, the shape of the fines portion of the curve, the amount of fine, and the diameter of the minimum allowable size particle. These model coefficients are difficult to obtain and lead to difficulties in the study of PSD. Hence, a mathematical model for tailings material PSD with fewer model coefficients will benefit CTB research.

The present study aims to build a mathematical model of tailings material using twelve different tailings sources from various mines in China. Loop iteration was used to obtain a more reliable model function to express the characteristics of particle size compositions with three coefficients. The model could then be validated using the twelve different tailings materials and was further applied in industrial applications.

2. Materials

Twelve different tailings sources from various mines in China were used in this study and each of them are conform to Non-hazardous industrial solid waste standard [48]. The tailings include coarse-grained tailings to extremely fine-grained tailings, representing the typical particle size distribution (PSD) range of tailings materials in underground metal mines. After sampling, the particle size distribution (PSD) of the used tailings were determined by Laser Particle Size Analyzer (PSA) (Malvern Mastersizer 2000: Malvern Instruments Ltd., Malvern, UK) and the specific gravity (ρ_s) of each tailing was measured [49]. As shown in Table 1, the measured particle size distribution and specific gravity for all twelve tailings were listed.

Table 1. The particle size distribution and specific gravity of tailings.

Samples	ρ_s	PSD Measured Curve, µm					
		d_{10} (1)	d_{30} (2)	d_{50} (3)	d_{60} (4)	d_{70} (5)	d_{90} (6)
Classified fine Copper tailing: S1	3.02	1.76	6.41	14.42	20.43	28.71	64.62
Unclassified Copper tailing: S2	2.64	2.25	9.34	36.27	56.83	81.42	172.7
Unclassified Copper-Nickel tailing: S3	2.94	2.62	10.56	27.94	42.53	62.52	132.48
Unclassified Polymetallic tailing: S4	3.19	2.75	12.86	33.71	53.15	82.34	203.57
Unclassified Copper tailing: S5	2.87	2.75	13.15	39.58	68.51	116.14	251.02
Unclassified Copper tailing: S6	2.75	2.95	11.78	28.97	43.56	65.03	151.48
Unclassified Copper tailing: S7	2.98	3.31	23.54	78.86	119.77	179.22	393.43
Unclassified Copper-Gold tailing: S8	2.95	4.44	11.1	21.88	31.21	45.9	118.76
Unclassified Copper-Gold tailing: S9	2.94	7.24	40.4	76.42	99.45	130.37	268.87
Unclassified Copper tailing: S10	2.96	9.31	46.57	82.46	105.45	137.32	284.11
Unclassified Iron tailing: S11	2.84	10.22	42.7	79.81	104.39	137.8	296.31
Classified coarse Copper tailing: S12	2.94	13.62	60.82	106.92	137.79	179.24	345.65

(1) The portion of particles with diameters smaller than this value is 10%. (2) The portion of particles with diameters smaller than this value is 30%. (3) The portion of particles with diameters smaller than this value is 50%. (4) The portion of particles with diameters smaller than this value is 60%. (5) The portion of particles with diameters smaller than this value is 70%. (6) The portion of particles with diameters smaller than this value is 90%.

Figure 1 illustrates the particle size distribution of all twelve tailings materials in semi-logarithmic coordinate space. S1 is the finest material used in this study in the twelve tailings, which is the classified fine part, followed by unclassified tailings S2 to S11 sourced from different metal mines and classified coarse tailing S12. Hence, the tailings materials from S1 to S12 are gradually coarsened, and the average grain size increases.

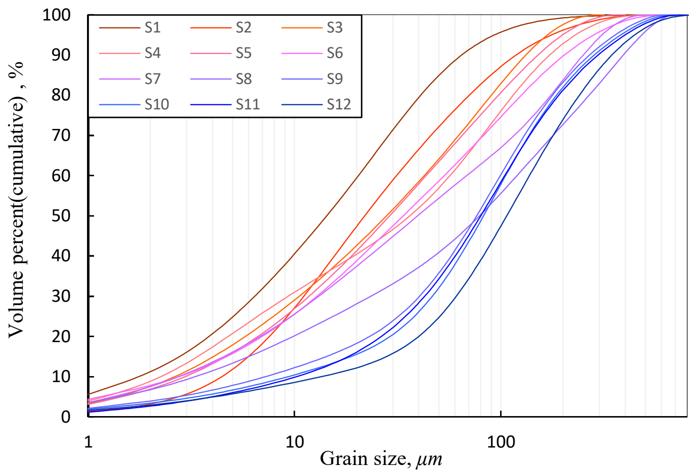

Figure 1. The particle size distribution of twelve different tailings.

3. Mathematical Model

3.1. Definition of Coefficients

As shown in Figure 1, the PSD of tailings on the logarithmic curve has S-shaped characteristics. The ordinate is the cumulative percentage value passing a specific particle size, and the abscissa is the logarithm of the particle diameter. Therefore, to establish a Mathematical Model for PSD of the tailings material, a Sigmoid function can be used to simulate the tailing's grain size distribution characteristics, as shown in Equation (1). The following contents will discuss further analysis by the goodness-of-fit test for its reliability.

$$N_i = \frac{K}{1 + A{X_i}^B} \tag{1}$$

where N_i refers to the cumulative percentage value of particles less than specific particle size, X_i, and A, B, K are the model coefficients.

The equivalent form of Equation (1) could be written as follows:

$$\ln(A) + B\ln(X_i) = \ln(\frac{K}{N_i} - 1) \tag{2}$$

The independent variable and dependent variable of Equation (2) can be equivalent, and then the equation could be modified as follows:

$$\overline{A} + B\overline{X} = \overline{Y} \tag{3}$$

where

$$\begin{cases} \overline{A} = \ln(A) \\ \overline{X_i} = \ln(X_i) \\ \overline{Y_i} = \ln(\frac{K}{N_i} - 1) \end{cases}$$

The model coefficients A, B and K in Equation (1) then can be obtained in the following steps:

Step 1: Three methods to determine Coefficient K

(a). Method 1: The meaning of K value is the cumulative fraction of particles when the particle size reaches infinity. Therefore, the approximate value is Approach to 100%. It is means K = 100 (Excluding percent sign, the same below).

(b). Method 2: According to Equation (2), three equidistant points are selected to eliminate the coefficients A and B. The value K can be calculated by solving the Equation (4). The equidistant points can be 37 μm, 74 μm, and 150 μm.

$$K = \frac{N_1[2N_0N_2 - N_1(N_0 + N_2)]}{N_0N_2 - N_1^2} \tag{4}$$

where N_0, N_1, and N_2 are the cumulative percentage values of particles passing 37 μm, 74 μm, and 150 μm. It should be pointed out that the K value can be calculated for N_0, N_1 and N_2 of any equidistant points. The above value method can cover most of the particle size range of tailings for common tailings, and the value is relatively reasonable.

(c). Method 3: The K value is optimal fitting solved by loop iterative calculation, which will be discussed in Section 3.2.

Step 2: Take points and linear regression to obtain coefficients A and B

The coefficients A and B can be obtained by linear regression of the measured tailing's particle size distribution scatters by Equation (3). A series of representative points are taken for regression analysis. In the present work, d_{10}, d_{30}, d_{50}, d_{60}, d_{70}, d_{90} are proposed. The linear regression equation could be written as follows:

$$\begin{cases} \overline{A} = \frac{\sum X_iY_i - \frac{1}{N}\sum X_i \sum Y_i}{\sum X_i^2 - \frac{1}{N}(\sum X_i)^2} \\ \overline{B} = \frac{\sum Y_i - \overline{A}\sum X_i}{N} \end{cases} \tag{5}$$

where (X_i, Y_i) is the sample point, i.e., (d_{10},10), (d_{30},30), (d_{50},50), (d_{60},60), (d_{70},70), (d_{90},90), and N is the number of samples (N = 6 in this study). The coefficients A and B can be obtained by substitution with $\overline{A}$ and $\overline{B}$ in Equation (3).

Step 3: Error analysis

To further analyze the reliability of this regression model, the following goodness-of-fit test error analysis method is used:

$$R^2 = 1 - \frac{SSR}{SST} = 1 - \frac{\sum \left(\hat{Y}_i - Y_i\right)^2}{\sum \left(\overline{Y}_i - Y_i\right)^2} \tag{6}$$

where R^2 reflects the goodness-of-fitting, also known as Determinants of coefficients, the maximum value of R^2 is 1, and the closer the value to 1, the better the fitting is. Generally, it should not be less than 0.8. SST is the square sum of total deviations; SSR is the square sum of errors; $\hat{Y}_i$ is the predictive value of the model; and $\overline{Y}_i$ is the average value of samples.

Through the above steps, the S-curve model can be obtained, but the reliability of the model is greatly affected by the measuring points, and the reliability index of error analysis could be low. In order to solve this problem, a simple loop iteration calculation is carried out based on the goodness-of-fit to find the most suitable model coefficients.

3.2. Iterative Analysis for the Optimal Fitting Coefficient

In order to obtain a more reliable model function to express the characteristics of particle size composition, the three model coefficients (A, B and K) are obtained by loop iteration. Figure 2 illustrates the structure of the loop iterative control flow chart. As shown in Figure 2, Equation (6) is used as the discrimination function of the iterative loop, where the initial value of K is taken as 100, and the loop step is 1 ($K = K + 1$). The Coefficient A and B in each cycle step are obtained by Equation (5), the corresponding model calculation value is calculated by Equation (1), and the corresponding goodness-of-fit is calculated by Equation (6).

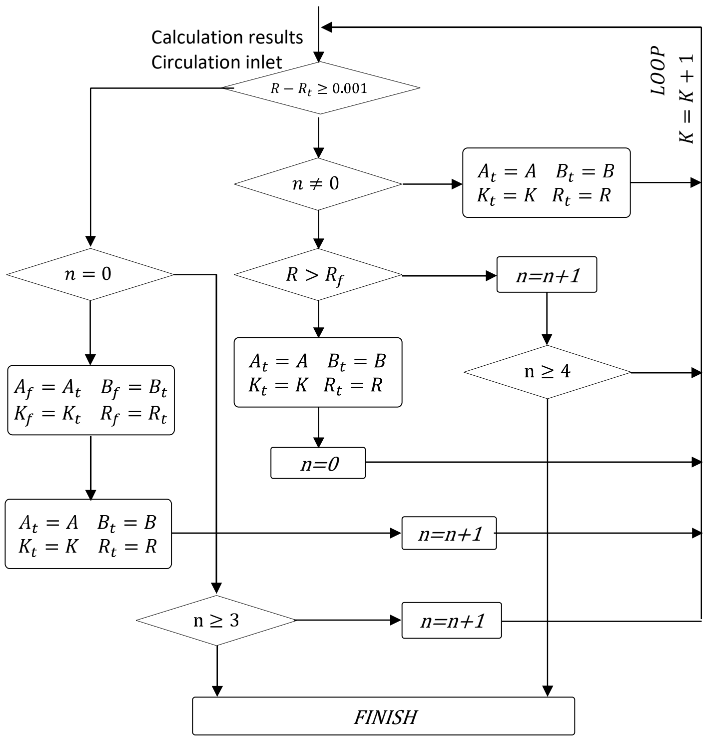

Figure 2. Loop iteration calculation method chart (Main loop idea: Set the circulation step of K value as 1.0, and calculate the A and B values according to the measured points. If the fitting coefficient R^2 of the model is greater than 0.99, it is regarded as the potential solution, and the potential solution appears three times in a row is the optimal solution, otherwise the output failures.).

At the starring of loop interactive, the initial value of K was taken as 100, the characteristic points (d_{10},10), (d_{30},30), (d_{50},50), (d_{60},60), (d_{70},70), (d_{90},90) as the sample points for linear regression were obtained, and the model coefficients A and B were calculated according to Equation (3). When the corresponding model calculation value $\hat{N}_i$ of the cumulative proportion of particles is calculated by Equation (1), R^2 can then be obtained by Equation (6). If R^2 satisfies the condition of loop termination, the calculation ends by increasing K by 1 for a new loop until the R^2 fits the loop termination requirements. The final values of model coefficients could finally be outputted. In this study, the condition for cycle terminations is $R^2 \leq 0.99$. Generally, the PSD model with enough goodness-of-fit can be obtained through a few loop-steps

3.3. Coefficients Interpretation

The three coefficients of the model determine the distribution characteristics of the particle size, each of them is analyzed as follows.

(a) Coefficient A reflects the average particle size

We plot the model curves with various A values for 10 to 100 when K = 100 and $B = -1.0$ as shown in Figure 3. The PSD curves move towards a coarse particle area with the increase, indicating that the Coefficient A is positively correlated with the overall particle size. Hence, the larger the value of A is, the larger the average particle size is, and vice versa.

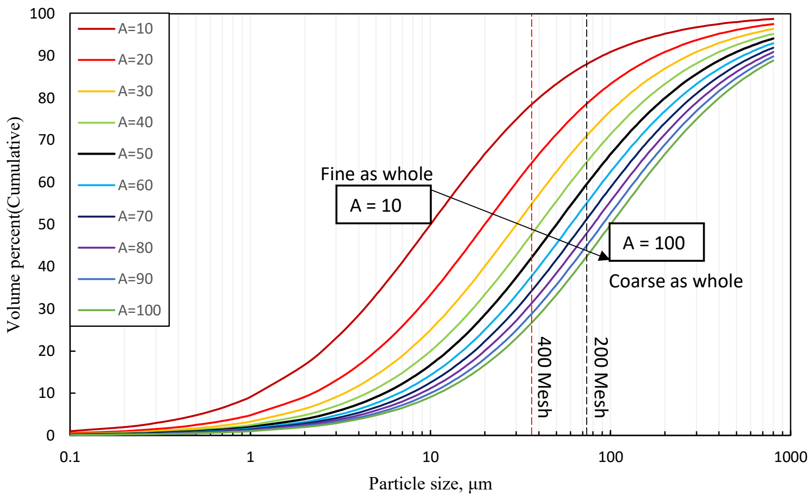

Figure 3. Model curve under different coefficient A.

(b) Coefficient B represents the proportion of coarse and fine tailings

Similarly, Figure 4 illustrates the model curves under different coefficient B values for -1.25 increasing to -0.8 when A = 50, K = 100. As shown in Figure 4, the fine fraction content increased in the particle size distribution with an increase in the B value. Therefore, the Coefficient B can reflect the proportion of the fine part to the coarse. The larger that B is, the smaller the fine particles contained, and vice versa.

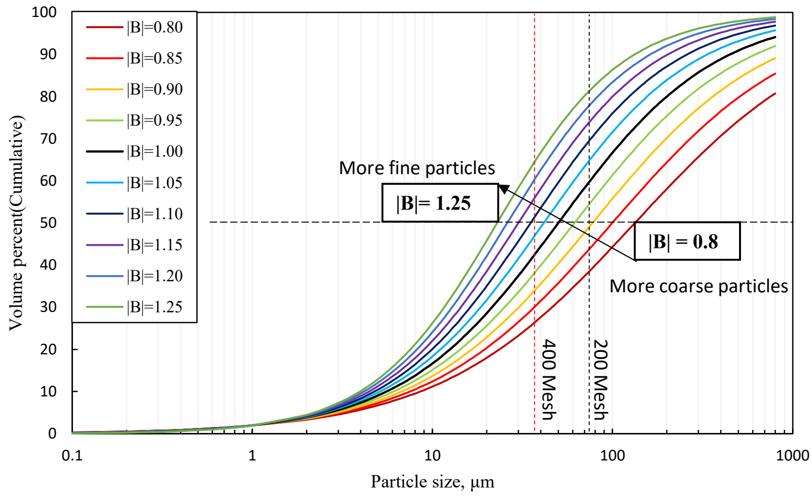

Figure 4. Model curve under different coefficient *B*.

(c) Coefficient *K* represents the width of particle distribution

Similarly, Figure 5 illustrates the modeled curve under different coefficients *K* increasing from 100 to 145 when A = 50 and B = −1.0. As shown in Figure 5, with the increase of *K*, the cumulative volume fraction of particles reaches 100% rapidly, and the corresponding particle size decreases significantly, which indicates that the Coefficient *K* can represent the maximum particle size and the distribution width of particles. The higher the *K* value is, the smaller the maximum particle size is and the narrower the particle distribution width, and vice versa.

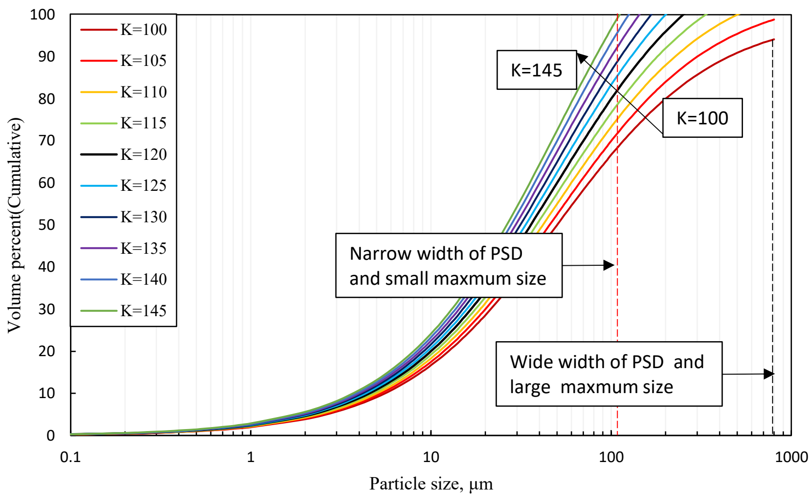

Figure 5. Model curve under different Coefficient *K*.

4. Validation and Discussion

Twelve kinds of tailings are used for verification. The coefficients of sample materials are shown in Table 1. The model is established by cyclic iteration, as described in Section 3. The results are shown in Table 2.

Coefficient *A* reflects the average fineness of tailings particles, as shown in Table 1, with the increase of samples number, the average particles sizes show an increasing trend; A = 19.32 for S1 sample, which is the smallest one, indicating that the sample is the finest tailings, A = 234.78 for S12, which is the largest one, indicating that the sample is the coarsest tailings. Coefficient *B* reflects the portion of coarse and fine tailings, as shown in Table 1, B = −0.69 of S8 sample is the largest, indicating the fine part proportion is the least, B = −1.29 of S2 sample is the smallest, indicating the fine part proportion is the most. Coefficient K reflects the width of PSD, as shown in Table 1, K = 101 of S2 sample is the lowest, indicating the distribution of PSD is the broadest, K = 126 of S8 sample is the highest, indicating the distribution of PSD is the narrowest.

Table 2. Tailings sample PSD model and coefficients.

Samples	Model	Coefficients			
		A	B	K	R^2
S1	$N_{\mathrm{i}} = \frac{104}{1+19.32e^{-1.12}}$	19.32	−1.12	104	0.999
S2	$N_{\mathrm{i}} = \frac{101}{1+57.78e^{-1.29}}$	57.78	−1.29	101	0.999
S3	$N_{\mathrm{i}} = \frac{120}{1+25.15e^{-0.87}}$	25.15	−0.87	120	0.999
S4	$N_{\mathrm{i}} = \frac{115}{1+19.57e^{-0.79}}$	19.57	−0.79	115	0.994
S5	$N_{\mathrm{i}} = \frac{109}{1+28.79e^{-0.96}}$	28.79	−0.96	109	0.999
S6	$N_{\mathrm{i}} = \frac{108}{1+25.18e^{-0.89}}$	25.18	−0.89	108	0.999
S7	$N_{\mathrm{i}} = \frac{116}{1+22.6e^{-0.77}}$	22.60	−0.77	116	0.996
S8	$N_{\mathrm{i}} = \frac{126}{1+27.98e^{-0.69}}$	27.98	−0.69	126	0.995
S9	$N_{\mathrm{i}} = \frac{115}{1+90.63e^{-1.0}}$	90.63	−1.00	115	0.995
S10	$N_{\mathrm{i}} = \frac{115}{1-133.67e^{-1.07}}$	133.67	−1.07	115	0.995
S11	$N_{\mathrm{i}} = \frac{108}{1+167.68e^{-1.16}}$	167.68	−1.16	108	0.997
S12	$N_{\mathrm{i}} = \frac{104}{1-19.32e^{-1.12}}$	234.78	−1.13	114	0.993

Overall, the model coefficients A, B, and K could well describe the average particle sizes, portion of coarse and fine tailings and the range for the particle size distribution. Figure 6 illustrates the semi-logarithmic PSD of all twelve samples modeled using the three coefficients, and their PSD characteristics are highly consistent with the measured PSD graph shown in Figure 1.

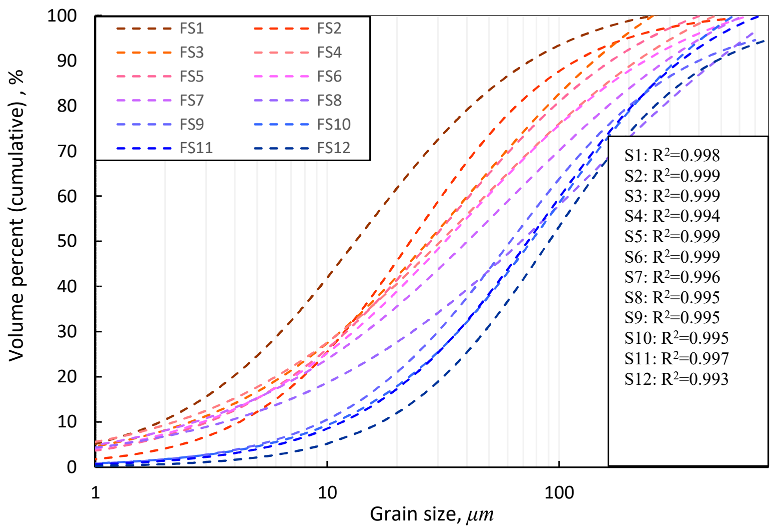

Figure 6. Model curve of tailings samples.

We compared the model curve with the measured curve and selected the particle size characteristic curves of two samples (S1 and S2) for a clear representation, in which the solid line is the measured PSD, and the dotted line is the model calculated PSD.

It can be seen from Figure 7, although there is a slight deviation in some local places of the curve, that the overall modeled curve is highly consistent with the measured one, which vividly reflects the fact of a high goodness-of-fit (R^2). Similarly, other samples also have the same regular characteristics, but due to the limited space, it will not be shown one by one.

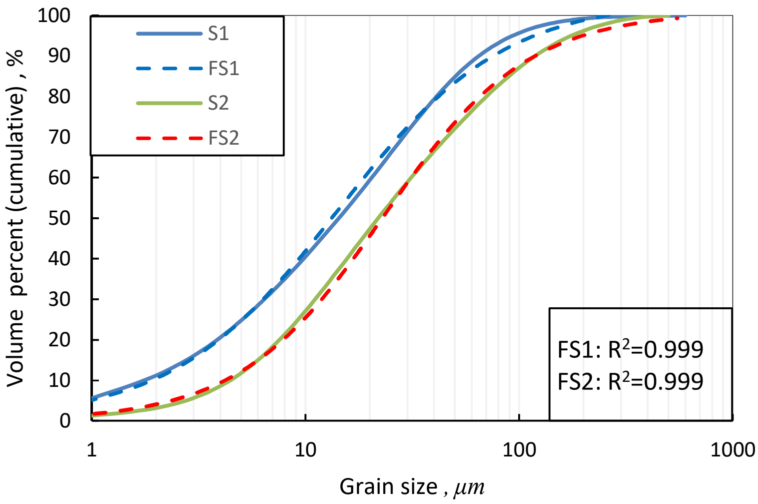

Figure 7. Comparison between modeled PSD curve and measured PSD curve.

5. Conclusions

This study firstly presents a mathematical model for the particle size distribution of mine tailings. The model contains three model coefficients (*A*, *B* and *K*) which mainly reflect the characteristics of particles from three aspects respectively, the average size of particles can be reflected by coefficient *A*, the proportion of the coarse or the fine parts of particles can be reflected by coefficient *B*, and the distribution width of particles can be reflected by coefficient *K*. Loop iteration was used to obtain a more reliable model function to express the characteristics of particle size composition with the three coefficients. Twelve tailing materials sourced from metal mines around China were used for the model establishment and validation. The goodness-of-fitting was given by R^2 for all twelve samples, each of them was greater than 0.99, showing a highly consistent between the test values and the model calculate values.

Compared with other particle characterization methods, using the proposed model to research the PSD features of tailings can intuitively obtain the overall particle size, the proportion characteristics tailings of coarse parts to fine parts, the distribution width of the particle size, which can provide a reference for studying the PSD features and its influence on other physical quantities, such as the strength characteristics of cemented backfill and the flow pattern characteristics of tailings slurry. This model is mainly focused on artificially grinded tailing materials in mineral procession, its applicability for natural formed particles such as sand or soil need be verified and the application on artificial sand such as construction sand, slag powder could be further studied.

Author Contributions: Conceptualization, Z.L.; Data curation, Y.Z.; Formal analysis, Z.L. and Y.Z.; Funding acquisition, L.G.; Investigation, Y.Z. and X.P.; Methodology, Z.L. and K.K.; Resources, L.G.; Validation, X.P.; Writing—original draft, Z.L.; Writing—review and editing, L.G. and K.K. All authors have read and agreed to the published version of the manuscript.

Funding: This research was supported by the National Key R&D Program of China (No. 2021YFC2900600, No. 2021YFE0102900); This research was also funded by the Key Research Fund of BGRIMM (No. 02-1911, 04-2208).

Data Availability Statement: The original contributions presented in the study are included in the article, and further inquiries can be directed to the corresponding authors.

Conflicts of Interest: The authors declare that the research was conducted in the absence of any commercial or financial relationships that could be construed as a potential conflict of interest.

References

1. Jones, H.; Boger, D.V. Sustainability and Waste Management in the Resource Industries. *Ind. Eng. Chem. Res.* **2012**, *51*, 10057–10065. [CrossRef]
2. Franks, D.M.; Boger, D.V.; Côte, C.M.; Mulligan, D.R. Sustainable development principles for the disposal of mining and mineral processing wastes. *Resour. Policy* **2011**, *36*, 114–122. [CrossRef]
3. Sivakugan, N.; Veenstra, R.; Naguleswaran, N. Underground Mine Backfilling in Australia Using Paste Fills and Hydraulic Fills. *Int. J. Geosynth. Ground Eng.* **2015**, *1*, 18. [CrossRef]
4. Birat, J.-P. Society, Materials, and the Environment: The Case of Steel. *Metals* **2020**, *10*, 331. [CrossRef]
5. El-Batsh, H.M.; Doheim, M.A.; Hassan, A.F. On the application of mixture model for two-phase flow induced corrosion in a complex pipeline configuration. *Appl. Math. Model.* **2012**, *36*, 5686–5699. [CrossRef]
6. Behera, S.K.; Mishra, D.; Singh, P.; Mishra, K.; Mandal, S.K.; Ghosh, C.; Kumar, R.; Mandal, P.K. Utilization of mill tailings, fly ash and slag as mine paste backfill material: Review and future perspective. *Constr. Build. Mater.* **2021**, *309*, 125120. [CrossRef]
7. Ting, X.; Xinzhuo, Z.; Miedema, S.A.; Xiuhan, C. Study of the characteristics of the flow regimes and dynamics of coarse particles in pipeline transportation. *Powder Technol.* **2019**, *347*, 148–158. [CrossRef]
8. Mourinha, C.; Palma, P.; Alexandre, C.; Cruz, N.; Rodrigues, S.M.; Alvarenga, P. Potentially Toxic Elements' Contamination of Soils Affected by Mining Activities in the Portuguese Sector of the Iberian Pyrite Belt and Optional Remediation Actions: A Review. *Environments* **2022**, *9*, 11. [CrossRef]
9. Liu, Q.; Liu, D.; Tian, Y.; Liu, X. Numerical simulation of stress-strain behaviour of cemented paste backfill in triaxial compression. *Eng. Geol.* **2017**, *231*, 165–175. [CrossRef]
10. Zhao, Y.; Taheri, A.; Karakus, M.; Deng, A.; Guo, L. The Effect of Curing under Applied Stress on the Mechanical Performance of Cement Paste Backfill. *Minerals* **2021**, *11*, 1107. [CrossRef]
11. Xu, W.; Cao, P.; Tian, M. Strength Development and Microstructure Evolution of Cemented Tailings Backfill Containing Different Binder Types and Contents. *Minerals* **2018**, *8*, 167. [CrossRef]
12. Le, Z.-H.; Yu, Q.-L.; Pu, J.-Y.; Cao, Y.-S.; Liu, K. A Numerical Model for the Compressive Behavior of Granular Backfill Based on Experimental Data and Application in Surface Subsidence. *Metals* **2022**, *12*, 202. [CrossRef]
13. Öhlander, B.; Chatwin, T.; Alakangas, L. Management of Sulfide-Bearing Waste, a Challenge for the Mining Industry. *Minerals* **2012**, *2*, 1–10. [CrossRef]
14. Wu, D.; Yang, B.; Liu, Y. Pressure drop in loop pipe flow of fresh cemented coal gangue–fly ash slurry: Experiment and simulation. *Adv. Powder Technol.* **2015**, *26*, 920–927. [CrossRef]
15. Li, M.-Z.; He, Y.-P.; Liu, Y.-D.; Huang, C. Pressure drop model of high-concentration graded particle transport in pipelines. *Ocean Eng.* **2018**, *163*, 630–640. [CrossRef]
16. Wilson, K.C. Deposition limit nomograms for particles of various densities in pipeline flow. *Hydrotransport* **1979**, *1*, 1–12.
17. Kesimal, A.; Yilmaz, E.; Ercikdi, B.; Alp, I.; Deveci, H. Effect of properties of tailings and binder on the short-and long-term strength and stability of cemented paste backfill. *Mater. Lett.* **2005**, *59*, 3703–3709. [CrossRef]
18. Libos, I.L.S.; Cui, L. Effects of curing time, cement content, and saturation state on mode-I fracture toughness of cemented paste backfill. *Eng. Fract. Mech.* **2020**, *235*, 107174. [CrossRef]
19. Zhao, Y.; Taheri, A.; Karakus, M.; Chen, Z.; Deng, A. Effects of water content, water type and temperature on the rheological behaviour of slag-cement and fly ash-cement paste backfill. *Int. J. Min. Sci. Technol.* **2020**, *30*, 271–278. [CrossRef]
20. Peng, X.; Guo, L.; Liu, G.; Yang, X.; Chen, X. Experimental Study on Factors Influencing the Strength Distribution of In Situ Cemented Tailings Backfill. *Metals* **2021**, *11*, 2059. [CrossRef]
21. Wilson, K.C.; Clift, R.; Addie, G.R.; Maffett, J. Effect of broad particle grading on slurry stratification ratio and scale-up-ScienceDirect. *Powder Technol.* **1990**, *61*, 165–172. [CrossRef]
22. Guo, W.; Han, Y.; Gao, P.; Tang, Z. Effect of operating conditions on the particle size distribution and specific energy input of fine grinding in a stirred mill: Modeling cumulative undersize distribution. *Miner. Eng.* **2022**, *176*, 107347. [CrossRef]
23. Quezada, G.R.; Ramos, J.; Jeldres, R.I.; Robles, P.; Toledo, P.G. Analysis of the flocculation process of fine tailings particles in saltwater through a population balance model. *Sep. Purif. Technol.* **2020**, *237*, 116319. [CrossRef]
24. Guo, Z.; Qiu, J.; Jiang, H.; Zhang, S.; Ding, H. Improving the performance of superfine-tailings cemented paste backfill with a new blended binder. *Powder Technol.* **2021**, *394*, 149–160. [CrossRef]
25. Zanko, L.M.; Niles, H.B.; Oreskovich, J.A. Mineralogical and microscopic evaluation of coarse taconite tailings from Minnesota taconite operations. *Regul. Toxicol. Pharmacol.* **2008**, *52* (Suppl. 1), S51–S65. [CrossRef]
26. Uzi, A.; Levy, A. Flow characteristics of coarse particles in horizontal hydraulic conveying. *Powder Technol.* **2018**, *326*, 302–321. [CrossRef]
27. Zhang, B.; Xin, J.; Liu, L.; Guo, L.; Song, K.-I. An Experimental Study on the Microstructures of Cemented Paste Backfill during Its Developing Process. *Adv. Civ. Eng.* **2018**, *2018*, 1–10. [CrossRef]
28. Singh, J.P.; Kumar, S.; Mohapatra, S.K. Modelling of two phase solid-liquid flow in horizontal pipe using computational fluid dynamics technique. *Int. J. Hydrogen Energy* **2017**, *42*, 20133–20137. [CrossRef]
29. Qi, C.; Chen, Q.; Fourie, A.; Zhao, J.; Zhang, Q. Pressure drop in pipe flow of cemented paste backfill: Experimental and modeling study. *Powder Technol.* **2018**, *333*, 9–18. [CrossRef]

30. Wu, D.; Yang, B.; Liu, Y. Transportability and pressure drop of fresh cemented coal gangue-fly ash backfill (CGFB) slurry in pipe loop. *Powder Technol.* **2015**, *284*, 218–224. [CrossRef]
31. Li, M.; He, Y.; Liu, Y.; Huang, C. Effect of interaction of particles with different sizes on particle kinetics in multi-sized slurry transport by pipeline. *Powder Technol.* **2018**, *338*, 915–930. [CrossRef]
32. Lu, G.; Fall, M.; Yang, Z. An evolutive bounding surface plasticity model for early-age cemented tailings backfill under cyclic loading. *Soil Dyn. Earthq. Eng.* **2019**, *117*, 339–356. [CrossRef]
33. Liu, L.; Fang, Z.; Wu, Y.; Lai, X.; Wang, P.; Song, K.-I. Experimental investigation of solid-liquid two-phase flow in cemented rock-tailings backfill using Electrical Resistance Tomography. *Constr. Build. Mater.* **2018**, *175*, 267–276. [CrossRef]
34. Matoušek, V.; Chára, Z.; Konfršt, J.; Novotný, J. Experimental investigation on effect of stratification of bimodal settling slurry on slurry flow friction in pipe. *Exp. Therm. Fluid Sci.* **2022**, *132*, 110561. [CrossRef]
35. Zhang, J.; Cheng, L.; Yuan, H.; Mei, N.; Yan, Z. Identification of viscosity and solid fraction in slurry pipeline transportation based on the inverse heat transfer theory. *Appl. Therm. Eng.* **2019**, *163*, 114328. [CrossRef]
36. Adiguzel, D.; Bascetin, A. The investigation of effect of particle size distribution on flow behavior of paste tailings. *J. Environ. Manag.* **2019**, *243*, 393–401. [CrossRef]
37. US Department of Commerce. *NIST Recommended Practice Guide: Particle Size Characterization*; National Institute of Standards and Technology: Gaithersburg, MD, USA, 2001.
38. Zhu, J.; Wu, S.; Cheng, H.; Geng, X.; Liu, J. Response of Floc Networks in Cemented Paste Backfill to a Pumping Agent. *Metals* **2021**, *11*, 1906. [CrossRef]
39. Kaushal, D.R.; Sato, K.; Toyota, T.; Funatsu, K.; Tomita, Y. Effect of particle size distribution on pressure drop and concentration profile in pipeline flow of highly concentrated slurry. *Int. J. Multiph. Flow* **2005**, *31*, 809–823. [CrossRef]
40. Kaushal, D.R.; Thinglas, T.; Tomita, Y.; Kuchii, S.; Tsukamoto, H. CFD modeling for pipeline flow of fine particles at high concentration. *Int. J. Multiph. Flow* **2012**, *43*, 85–100. [CrossRef]
41. Lang, L.; Song, K.-I.; Lao, D.; Kwon, T.-H. Rheological Properties of Cemented Tailing Backfill and the Construction of a Prediction Model. *Materials* **2015**, *8*, 2076–2092. [CrossRef]
42. Pang, B.; Wang, S.; Liu, G.; Jiang, X.; Lu, H.; Li, Z. Numerical prediction of flow behavior of cuttings carried by Herschel-Bulkley fluids in horizontal well using kinetic theory of granular flow. *Powder Technol.* **2018**, *329*, 386–398. [CrossRef]
43. Jiang, F.; Zhao, P.; Qi, G.; Li, N.; Bian, Y.; Li, H.; Jiang, T.; Li, X.; Yu, C. Pressure drop in horizontal multi-tube liquid–solid circulating fluidized bed. *Powder Technol.* **2018**, *333*, 60–70. [CrossRef]
44. Arolla, S.K.; Desjardins, O. Transport modeling of sedimenting particles in a turbulent pipe flow using Euler–Lagrange large eddy simulation. *Int. J. Multiph. Flow* **2015**, *75*, 1–11. [CrossRef]
45. Fredlund, M.D.; Wilson, G.W.; Fredlund, D.G. Use of the grain-size distribution for estimation of the soil-water characteristic curve. *Can. Geotech. J.* **2002**, *39*, 1103–1117. [CrossRef]
46. Fredlund, M.D.; Fredlund, D.G. Prédiction of the soil-water characteristic curve from the grain-size distribution curve. In Proceedings of the 3rd Symposium on Unsaturated Soil, Rio de Janeiro, Brazil, 22–25 April 1997.
47. Fredlund, M.; Wilson, G.W.; Fredlund, D.G. Use of Grain-Size Functions in Unsaturated Soil Mechanics. In *Advances in Unsaturated Geotechnics*; American Society of Civil Engineers: Reston, VA, USA, 2000.
48. Standardization Administration. *Standard for Pollution Control on the Non-Hazardous Industrial Solid Waste Storage and Landfill*; State Administration for Market Regulation, Ed.; China Environmental Publishing Group: Beijing, China, 2021.
49. *D02.04.0D*; Standard Test Method for Density, Relative Density, and API Gravity of Liquids by Digital Density Meter (ASTM D4052-2009). ASTM: West Conshohocken, PA, USA, 2009.